

Supplement of The Cryosphere, 13, 281–296, 2019
<https://doi.org/10.5194/tc-13-281-2019-supplement>
© Author(s) 2019. This work is distributed under
the Creative Commons Attribution 4.0 License.



Supplement of

Estimation of the Antarctic surface mass balance using the regional climate model MAR (1979–2015) and identification of dominant processes

Cécile Agosta et al.

Correspondence to: Cécile Agosta (cecile.agosta@gmail.com)

The copyright of individual parts of the supplement might differ from the CC BY 4.0 License.

Table S1: References of snow density datasets. For each depth range, we give the total number of observations (left) and the number of 35×35 km model grid cells they cover (right).

Reference	Dataset	0–20 cm	0–50 cm	0–100 cm
Albert et al. (2007)	SUMup17 [1]	3/1	3/1	3/1
Brucker and Koenig (2011)	SUMup17 [1]	6/5	6/5	6/5
Cameron et al. (1968)	Kaspers04 [2]	0/0	0/0	22/22
Ding et al. (2011)	CHINARE	568/39	0/0	0/0
Fujiwara and Endo (1971)	JARE69	65/38	0/0	13/13
Gallet et al. (2011)	DC-DDU08	8/8	7/7	0/0
Herron and Langway (1980)	Kaspers04 [2]	0/0	1/1	1/1
Kaspers et al. (2004)	Kaspers04 [2]	0/0	2/2	2/2
Kreutz et al. (2011)	SUMup17 [1]	1/1	1/1	1/1
Medley et al. (2013)	SUMup17 [1]	1/1	3/3	2/2
Sugiyama et al. (2012)	JASE07	0/0	43/43	43/42
Watanabe (1975)	JARE70	6/1	6/5	8/5
van den Broeke et al. (1999)	Kaspers04 [2]	0/0	8/8	8/8

[1] [Montgomery et al. \(2018\)](#), [2] [Kaspers et al. \(2004\)](#)

Table S2: Estimates of drifting snow transport fluxes summed over the total (TIS, $13.4 \cdot 10^6$ km²) and the grounded (GIS, $12.0 \cdot 10^6$ km²) Antarctic ice sheet, excluding Peninsula. Parenthesis ($\alpha_{max}, w_{smin}, w_{smax}$) are for estimates of drifting snow transport based on a scaling of the curvature: drifting snow transport ($\text{kg m}^{-2} \text{yr}^{-1}$) = α ($10^6 \text{ kg m}^{-1} \text{yr}^{-1}$) \times curvature (10^{-6} m^{-1}), with $\alpha = 0$ ($10^6 \text{ kg m}^{-1} \text{yr}^{-1}$) for wind speed lower than w_{smin} (m s^{-1}), $\alpha = \alpha_{max}$ ($10^6 \text{ kg m}^{-1} \text{yr}^{-1}$) for wind speed greater than w_{smax} (m s^{-1}), and α linearly increasing as a function of wind speed in between. Wind speed is the annual average of 10 m wind speed of MAR forced by ERA-Interim.

Component	(3700,5,9)	(3700,6,8)	(4700,5,9)	(2700,5,9)	RACMO2
TIS w/o Peninsula					
Mass loss (Gt yr^{-1})	82	81	95	66	21
Mass gain (Gt yr^{-1})	74	74	88	58	16
Net (Gt yr^{-1})	8	7	7	8	5
GIS w/o Peninsula					
Mass loss (Gt yr^{-1})	81	80	94	65	19
Mass gain (Gt yr^{-1})	68	69	81	53	14
Net (Gt yr^{-1})	13	11	13	12	5

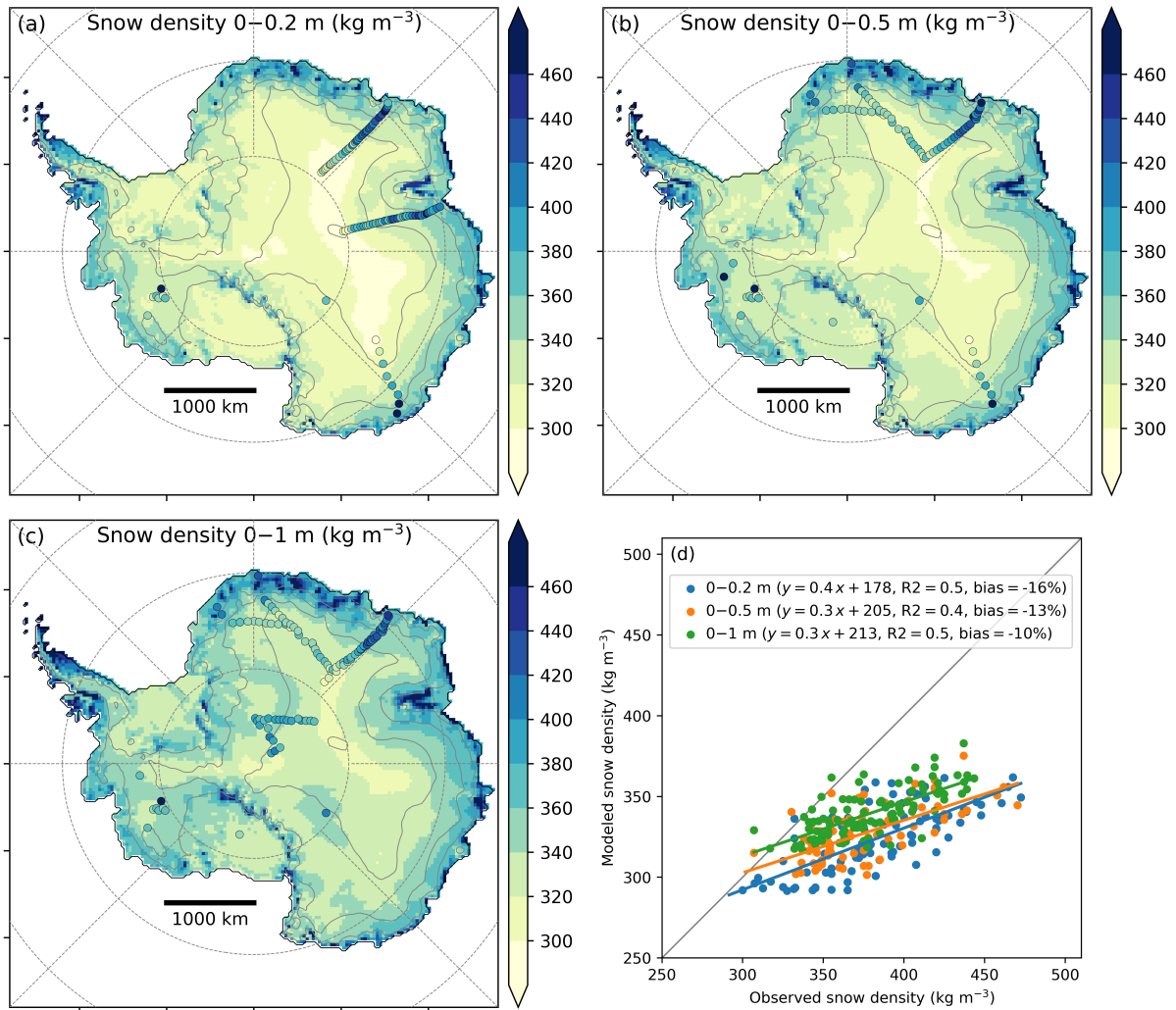


Figure S1: Snow density modelled by MAR (maps) and observations (dots) for (a) the first 20 cm of snow, (b) the first 50 cm of snow and (c) the first meter of snow, and (d) shows scatterplot of modelled versus observed snow density. The snow density database is detailed in Table S1. Modelled snow density is taken in average for the period 1979-2015. Observed snow density is averaged on MAR grid cells.

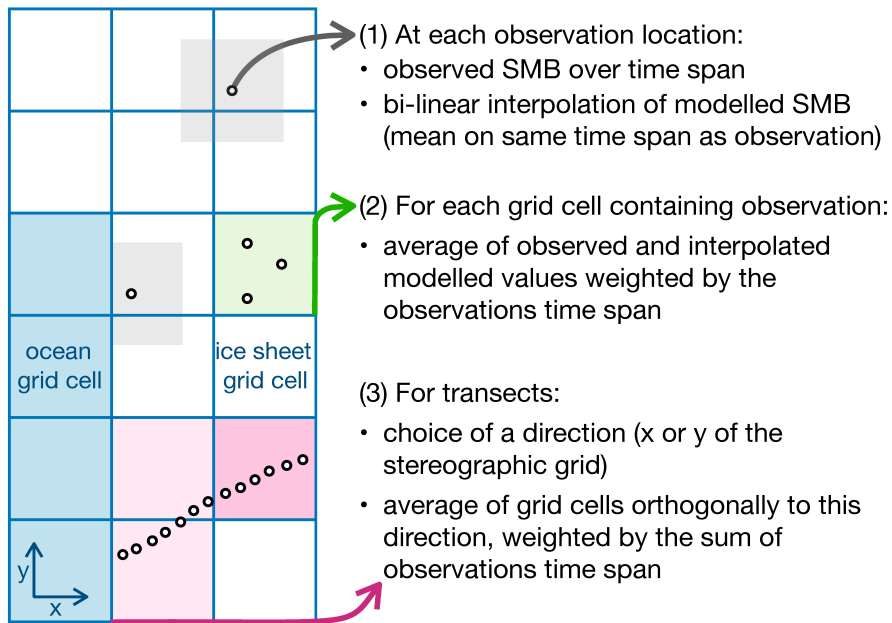


Figure S2: Sketch explaining the comparison method between observed (points) and modelled (gridded) SMB.

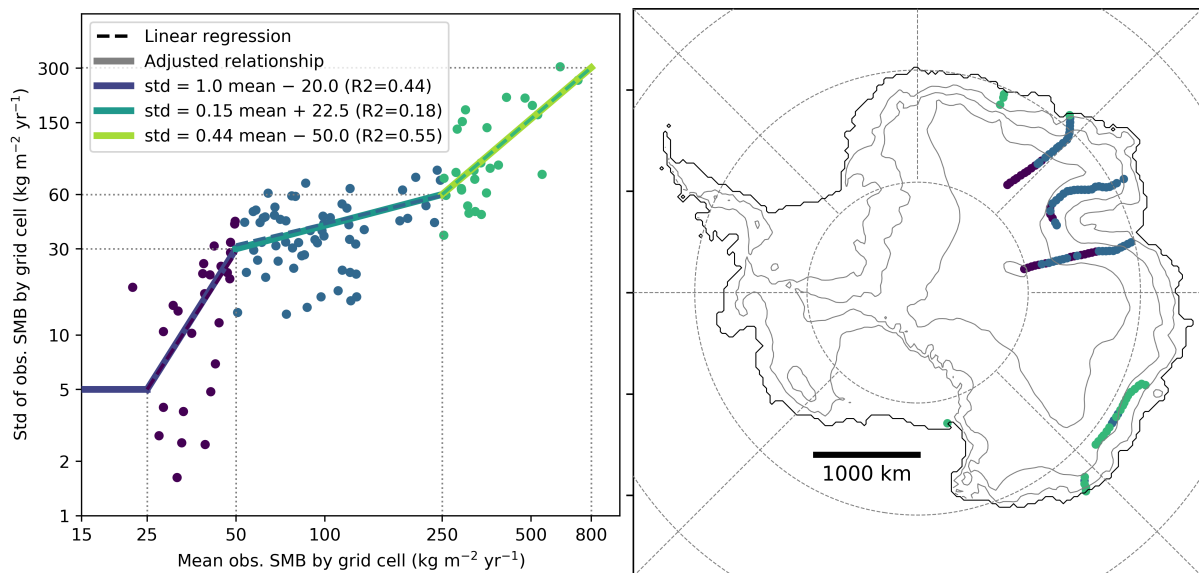


Figure S3: Estimate of the SMB spatial variability into $35 \text{ km} \times 35 \text{ km}$ grid cells as a function of mean observed SMB in the grid cell. (a) Standard deviation versus mean value of observed SMB for each MAR grid cell containing more than 10 observations. We delimitate three variability regimes depending on mean SMB values : $\leq 50 \text{ kg m}^{-2} \text{ yr}^{-1}$, $[50-250] \text{ kg m}^{-2} \text{ yr}^{-1}$ and $\geq 250 \text{ kg m}^{-2} \text{ yr}^{-1}$. (b) Location of the SMB regimes, with same colour code as in panel (a).

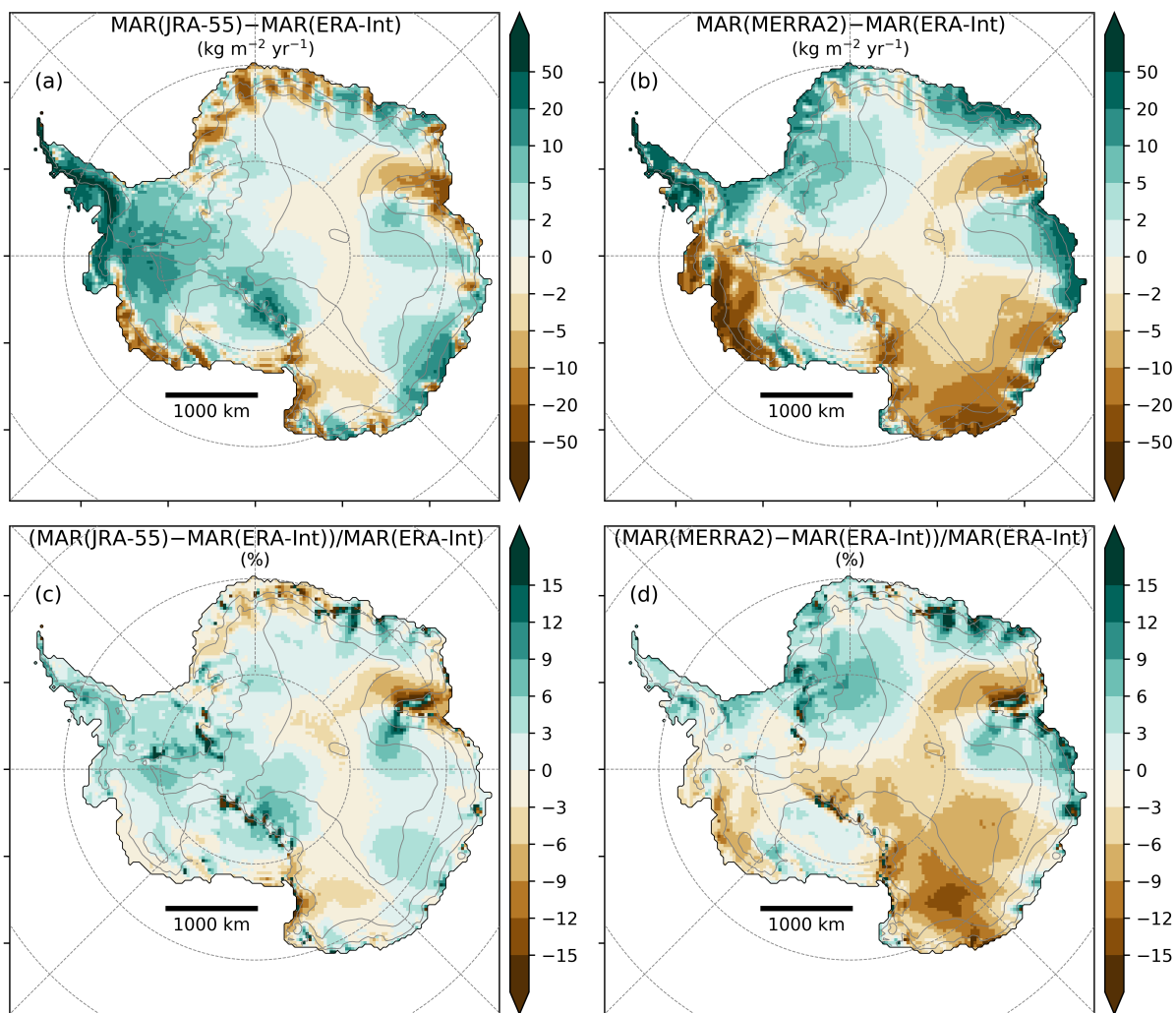


Figure S4: Difference between mean annual SMB modelled by MAR forced by (a) JRA-55 and (b) MERRA2 and MAR forced by ERA-Interim, for the period 1979-2015, in $\text{kg m}^{-2} \text{yr}^{-1}$. (c) and (d) are the same than (a) and (b) but divided by MAR(ERA-Interim) mean SMB (in %).

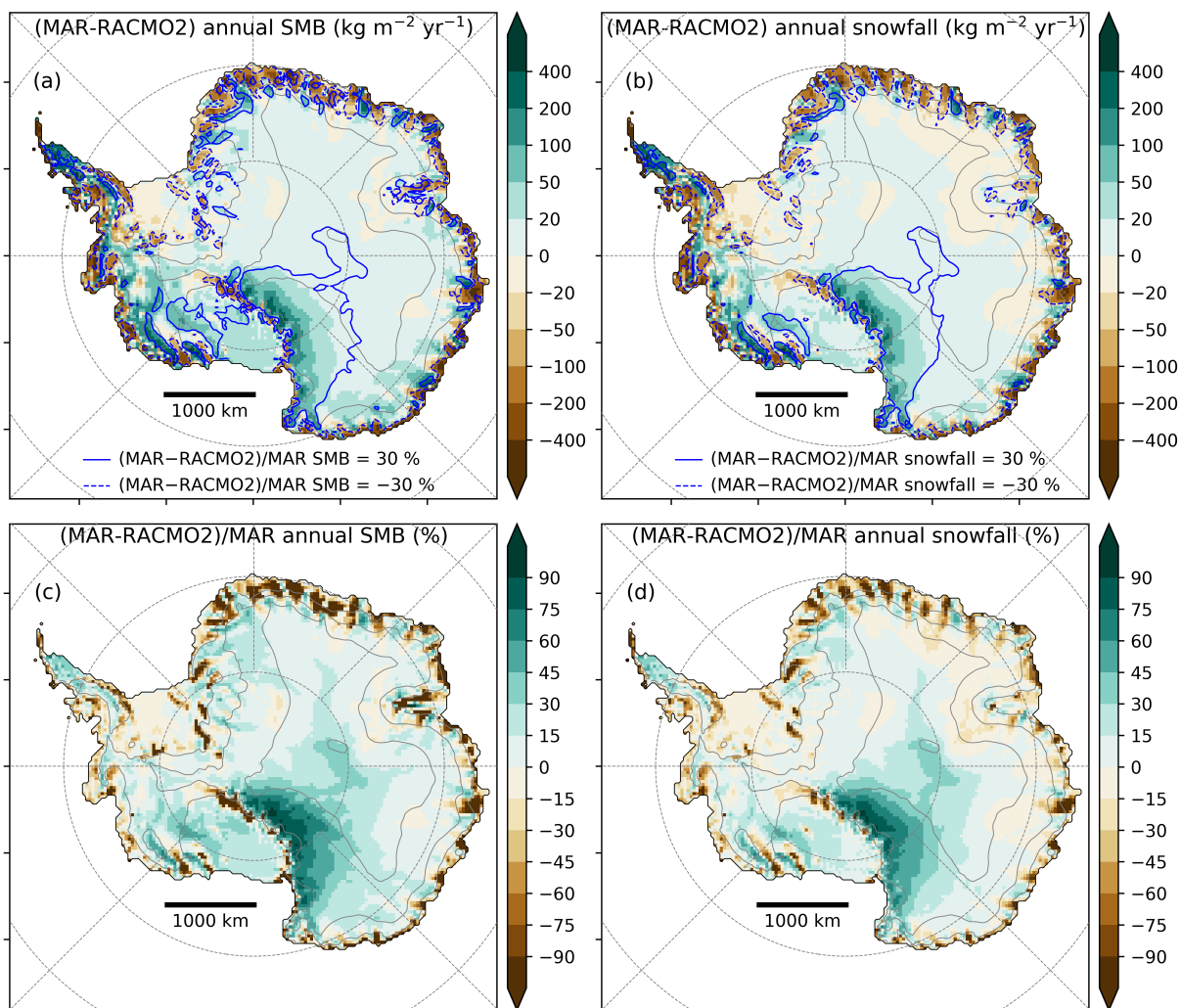


Figure S5: Difference between MAR and RACMO2 forced by ERA-Interim for the period 1979-2015 for (a-c) SMB and (b-d) snowfall. (a-b) Absolute differences, in $\text{kg m}^{-2} \text{yr}^{-1}$, and (c-d) relative differences, in $\%$. In (a-b), blue lines delimitate areas where the SMB/snowfall difference is 30 % greater than MAR SMB/snowfall, with solid lines when MAR is greater than RACMO2 and dashed lines when MAR is lower than RACMO2.

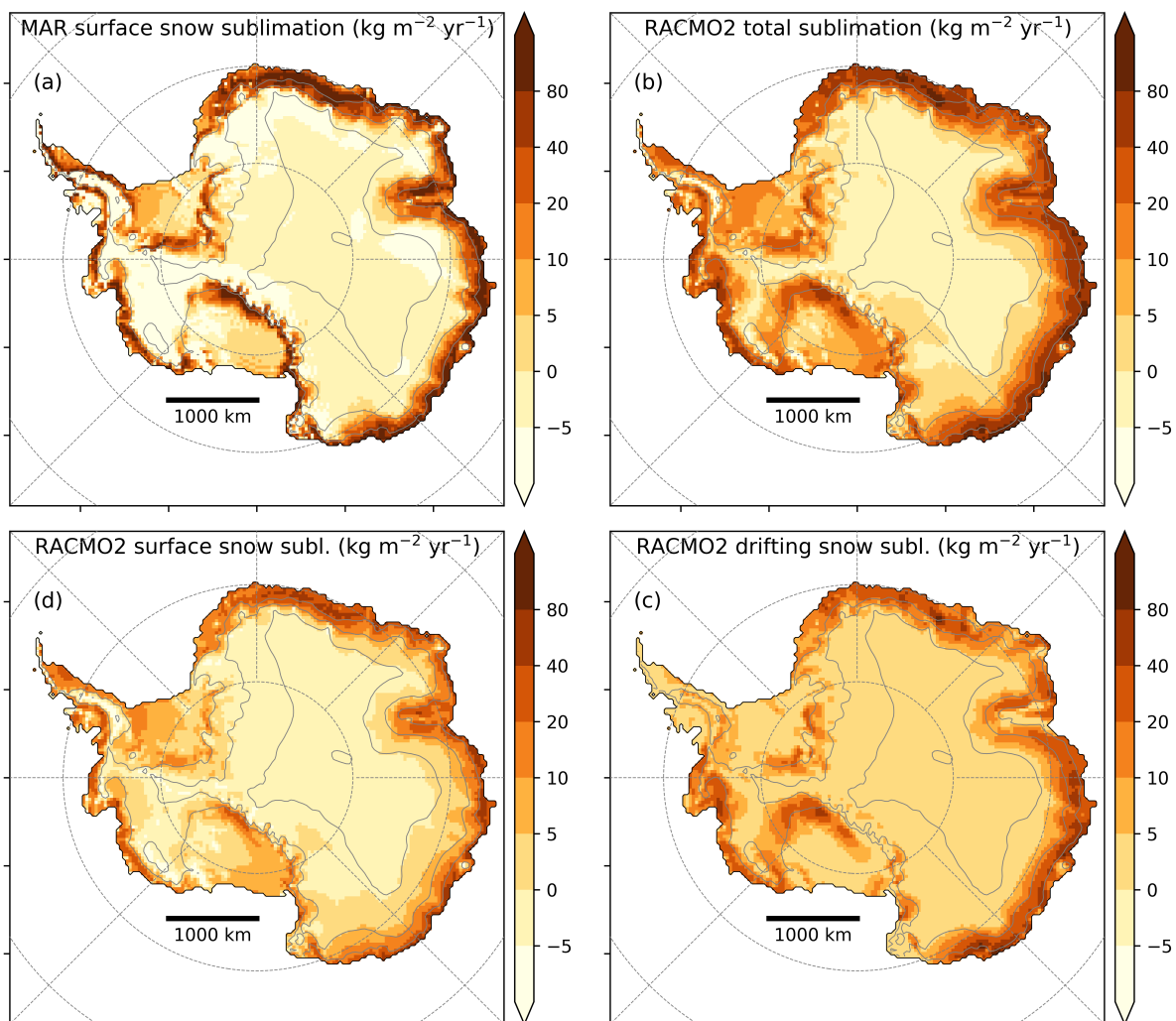


Figure S6: Annual mean modelled sublimation fluxes for the period 1979-2015, in $\text{kg m}^{-2} \text{yr}^{-1}$. (a) Sublimation at the surface of the snowpack modelled by MAR(ERA-Interim). (b) Total sublimation (surface snow sublimation plus drifting snow sublimation) modelled by RACMO2(ERA-Interim). (c) Same as (a) but for RACMO2(ERA-Interim). (d) Drifting snow sublimation modelled by RACMO2(ERA-Interim). MAR does not include drifting snow in these simulations.

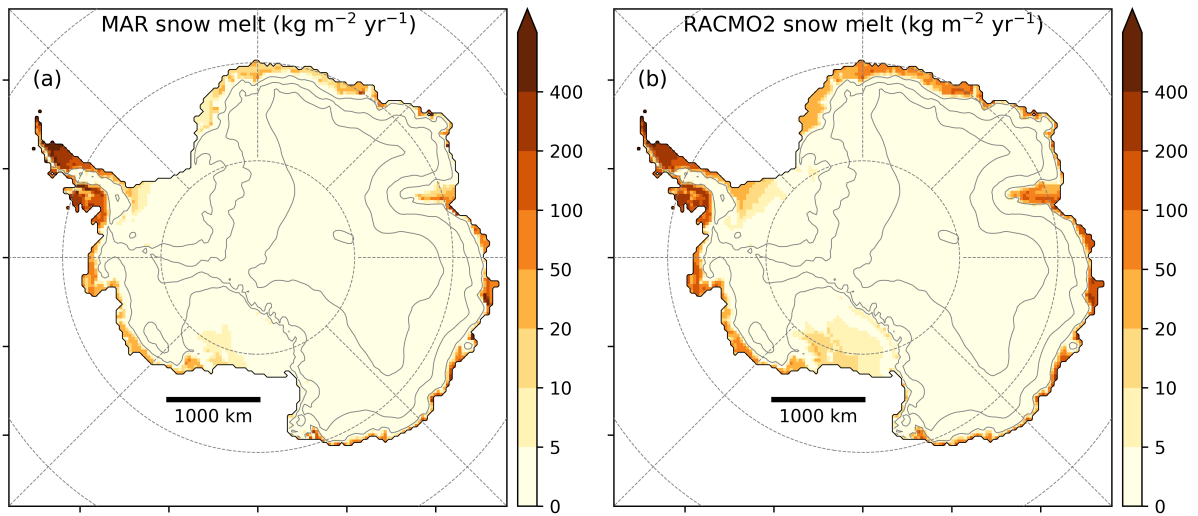


Figure S7: Snowmelt amounts modelled by MAR and RACMO2 forced by ERA-Interim for the period 1979-2015, in $\text{kg m}^{-2} \text{yr}^{-1}$. Note that snowmelt is almost totally refrozen in the snowpack in both models (Table 2).

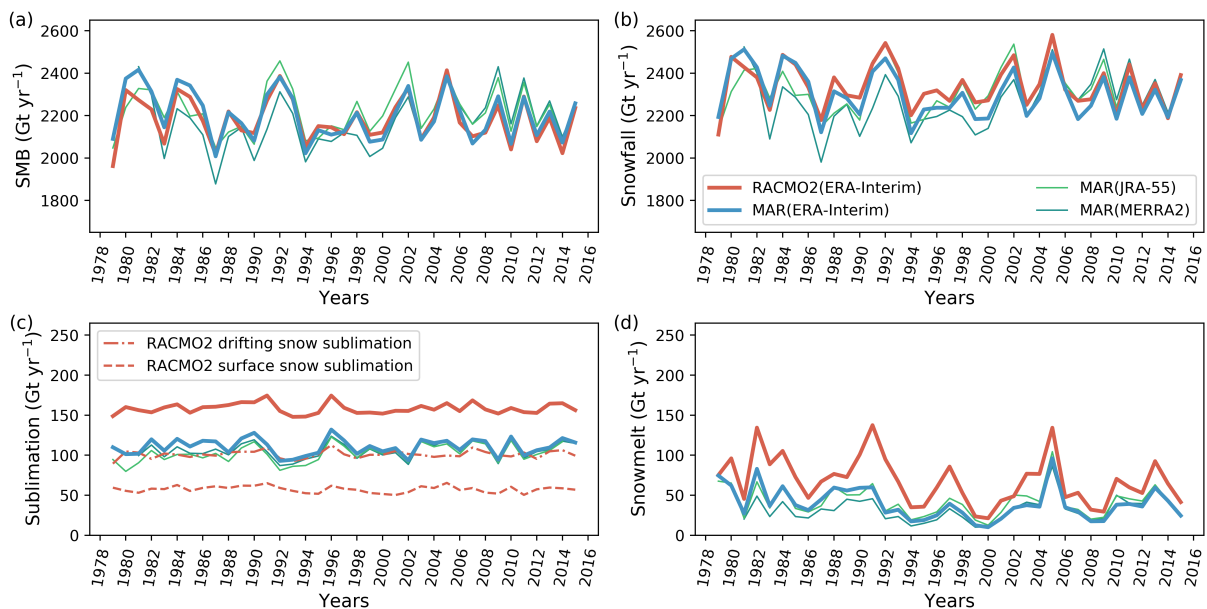


Figure S8: Annual SMB components summed over the Antarctic ice-sheet excluding peninsula ($13.4 \cdot 10^6 \text{ km}^2$), for (a) SMB, (b) snowfall, (c) sublimation and (d) snowmelt. Red solid thick line is for RACMO2(ERA-Interim), light green solid thin line is for MAR(ERA-Interim), blue solid thick line is for MAR(JRA-55) and dark green solid thin line is for MAR(MERRA2). Note that snowmelt is almost totally refrozen in the snowpack in both models (Table 2).

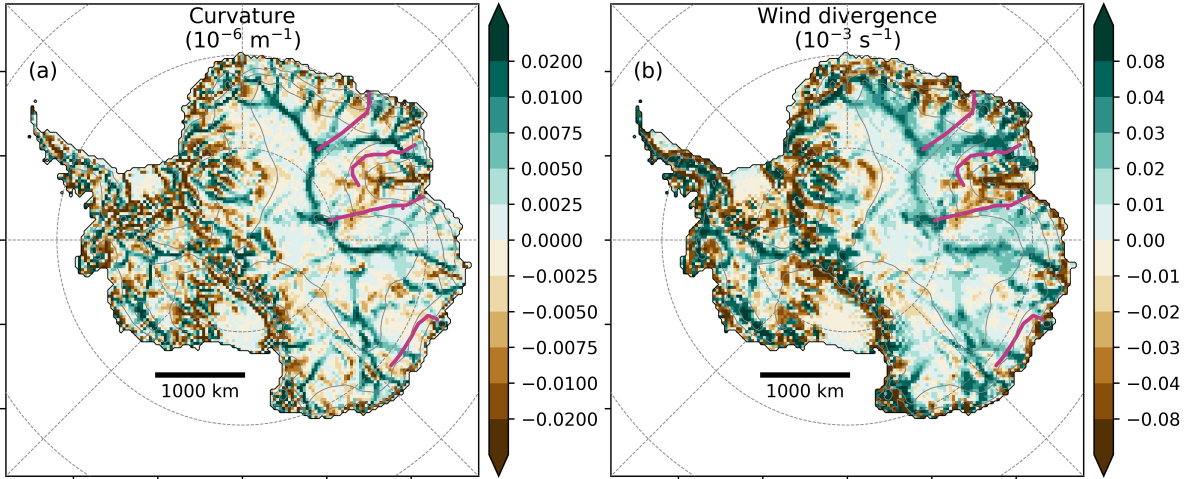


Figure S9: (a) Curvature of topography computed on the MAR grid (10^{-6} m^{-1}) (b) Divergence of the mean annual 10 m wind in MAR ($\text{m s}^{-1} \text{ km}^{-1}$)

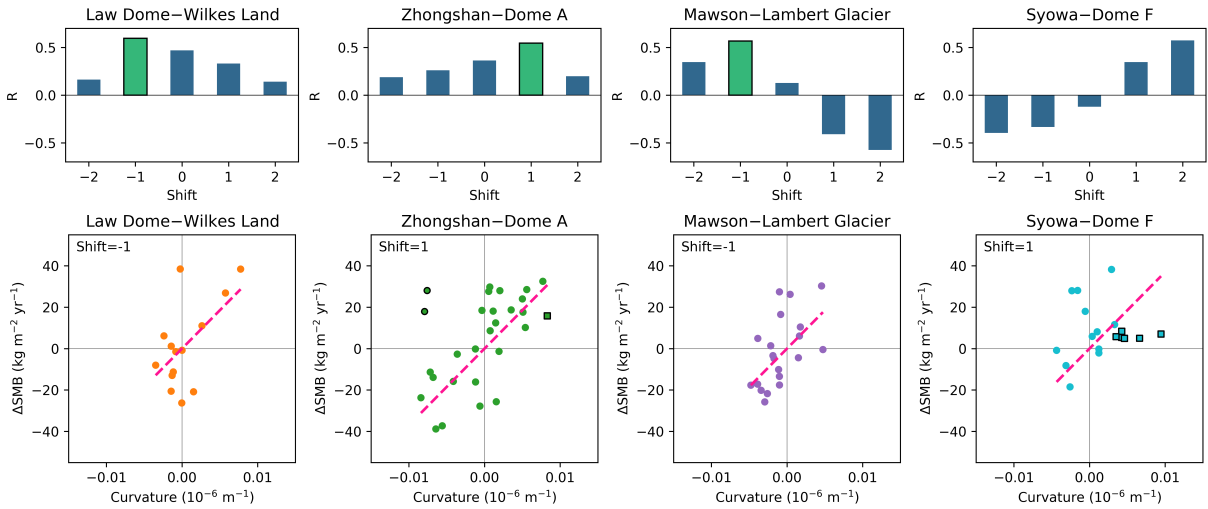


Figure S10: (top) Correlation coefficient R between MAR(ERA-Interim) SMB bias and curvature spatially shifted of -2, -1, 0, 1 and 2 grid cells. Green bars are for p -value lower than 0.05 and R greater than 0. (bottom) Scatterplots of MAR(ERA-Interim) SMB bias versus shifted curvature, with shift given at top left of each sub-figure. Pink dashed line is the regression line through origin computed for the four transects all-together (Fig. 4a). Squares are for locations where MAR annual 10 m wind speed is lower than 7 m s^{-1} . For the transect Zhongshan–Dome A, we excluded one data point with low wind speed (square with black outline) and two data points which were clear outliers (dots with black outlines). For the transect Syowa–Dome F, we excluded 5 data points with low wind speed (squares with black outlines).

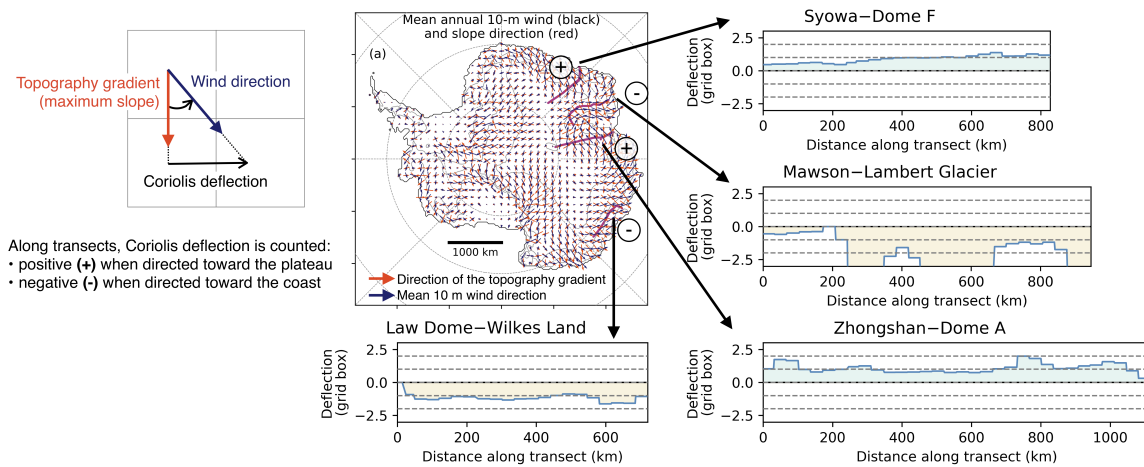


Figure S11: Estimate of the Coriolis deflection of the katabatic wind flow at the ice sheet surface. We compute the angle between the gradient of the topography (direction of the maximum slope) and the wind direction, and convert it in a deflection value, in percentage of the grid box size (deflection = $\tan(\text{angle})$). As transects are shown from the coast to the plateau, the Coriolis deflection sign is counted along this same axis: a deflection toward the coast shifts the wind backward in the axis (negative deflection), and a deflection toward the plateau shifts the wind upward in the axis (positive deflection). Finally, as curvature of the topography is used as a proxy of wind divergence which drives the drifting snow transport, the shift of curvature of +/- one grid cell according to the maximum of correlation with SMB bias (Fig. S10) is in agreement with the Coriolis wind deflection.

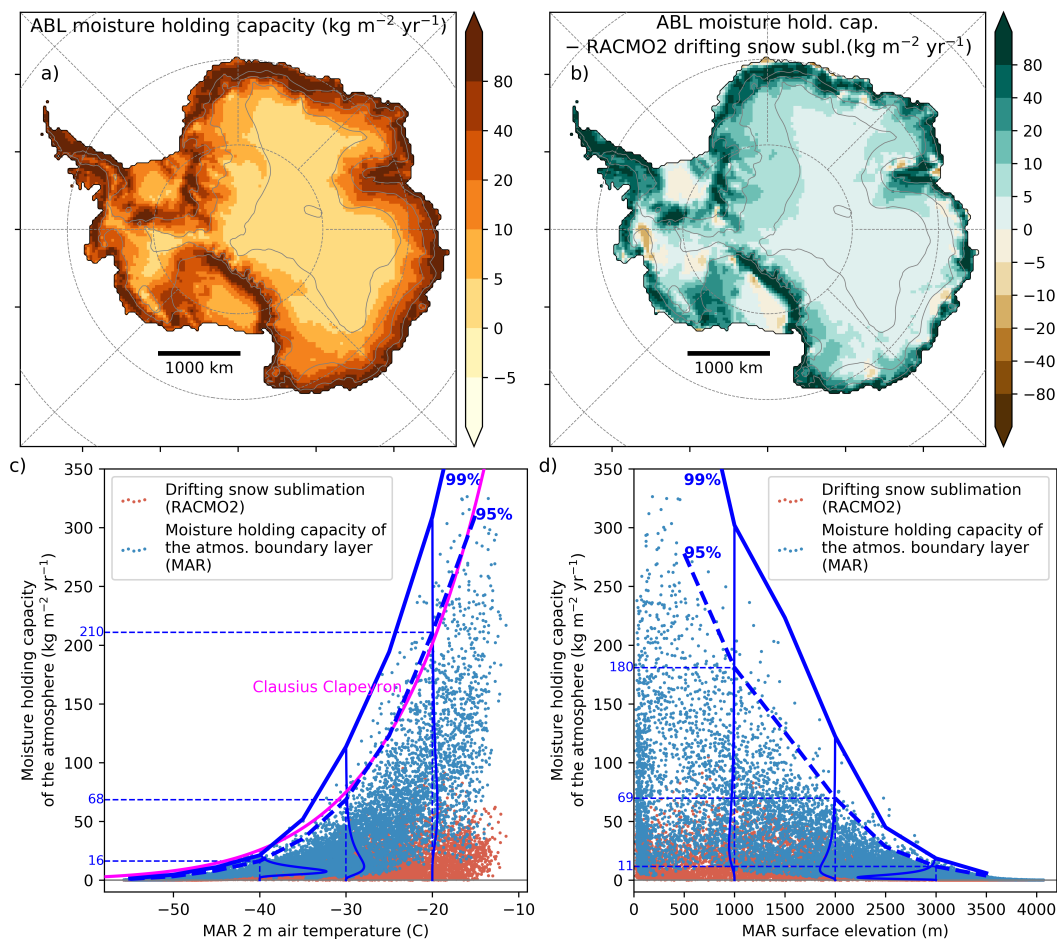


Figure S12: (a) Atmospheric boundary layer (ABL) moisture holding capacity in MAR for the year 2015, in $\text{kg m}^{-2} \text{yr}^{-1}$. The ABL moisture holding capacity is computed with daily variables: $\text{ABL moisture holding capacity} = \sum_{k=surface}^{k=ABLsummit} (Q_{sat} - Q) \Delta P / g$, with Q the specific humidity, Q_{sat} the specific humidity at saturation, ΔP the pressure width of the atmospheric layer k and g the gravitational acceleration. We compute the top of the ABL as the level where the turbulent kinetic energy amounts to 1% of the turbulent kinetic energy maximum in the lowest layers of the model (5% is used in Gallée et al., 2015). We compute Q_{sat} using the relative humidity rh : $Q_{sat} = Q / rh$. (b) Difference between the ABL moisture holding capacity in MAR and the drifting snow sublimation in RACMO2, for the year 2015, in $\text{kg m}^{-2} \text{yr}^{-1}$ (c) ABL moisture holding capacity in MAR (blue dots) and drifting snow sublimation in RACMO2 (red dots), for the year 2015, in $\text{kg m}^{-2} \text{yr}^{-1}$, as a function of the mean 2 m air temperature in MAR, for the year 2015, in $^{\circ}\text{C}$. The thin solid blue lines are normalised log-normal distribution of the ABL moisture holding capacity in MAR for 5 $^{\circ}\text{C}$ temperature bins around -40 $^{\circ}\text{C}$, -30 $^{\circ}\text{C}$, and -20 $^{\circ}\text{C}$. The thick blue dashed line shows the 95% end of the distributions, and the thick blue solid line is the 99% end of the distributions. The pink line shows a Clausius-Clapeyron-like relationship with temperature: $y = \exp(-L_s / R_v (1/ta - 1/ta_0) + \log(subl_0))$, in $\text{kg m}^{-2} \text{yr}^{-1}$, with ta the air temperature in K, L_s the enthalpy of sublimation ($2.8 \cdot 10^6 \text{ J kg}^{-1}$), R_v the gas constant of water vapor ($461.52 \text{ J kg}^{-1} \text{ K}^{-1}$), $ta_0 = 263.15 \text{ K}$ and $subl_0 = 500 \text{ kg m}^{-2} \text{yr}^{-1}$. (d) Same as (c) but for surface elevation instead of air temperature. Normalised distributions are computed for 500 m bins around 1000 m asl, 2000 m asl, and 3000 m asl. The ABL moisture holding capacity computed in the MAR model represents the maximum moisture amount that can be loaded in the atmospheric boundary layer according to the MAR simulations. We can confidently consider this ABL moisture holding capacity as an upper bound for drifting snow sublimation amounts (panels a and b), as MAR not including the drifting snow process implies that the ABL keeps its full potential to hold moisture. The ABL moisture holding capacity is exponentially dependent to the air temperature, following a Clausius-Clapeyron-like relationship (panel c).

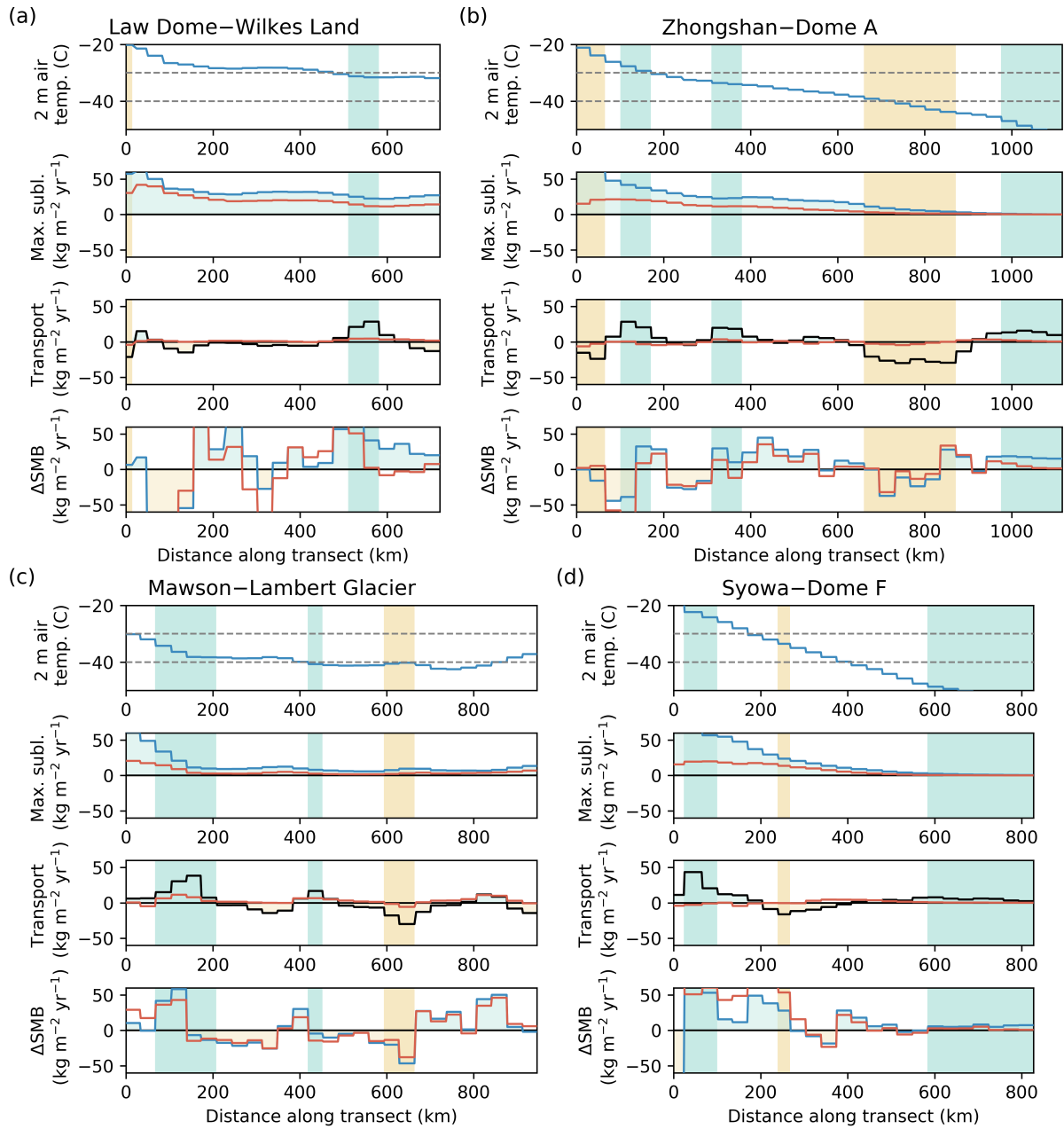


Figure S13: For each of the four long transects is shown, from top to bottom, for the year 2015: (top row) 2 m air temperature, in $^{\circ}\text{C}$; (2nd row) atmospheric boundary layer moisture holding capacity in MAR (blue line), and drifting snow sublimation in RACMO2 (red line), in $\text{kg m}^{-2} \text{yr}^{-1}$; (3rd row) drifting snow transport estimate as a function of curvature (black line), and drifting snow transport simulated by RACMO2 (solid red line), in $\text{kg m}^{-2} \text{yr}^{-1}$; (bottom row) the difference between modelled and observed SMB for MAR (blue line) and RACMO2 (red line), in $\text{kg m}^{-2} \text{yr}^{-1}$. The blue bands are when the curvature of the topography is greater than $0.004 \cdot 10^{-6} \text{ m}^{-1}$ (crests) and yellow bands are when the curvature of the topography is lower than $-0.004 \cdot 10^{-6} \text{ m}^{-1}$ (valleys).

References

- Albert, M. R., Courville, Z., and Cathles, M.: Snow and Firn Permeability: Characteristics of Snow Megadunes and their Potential Effects on Ice Core Interpretation, U.S. ANTARCTIC PROGRAM DATA CENTER, 2007.
- Brucker, L. and Koenig, L.: Satellite-Era Accumulation Traverse 2011 (SEAT11) snowpit density data , Unpublished, 2011.
- Cameron, R. L., Picciotto, E., Kane, H. S., and Gliozzi, J.: Glaciology of the Queen Maud Land Traverse, 1964-65 South Pole - Pole of Relative Inaccessibility, Research Foundation and the Institute of Polar Studies, The Ohio State University, 43212, 1968.
- Ding, M., Xiao, C., Li, Y., Ren, J., Hou, S., Jin, B., and Sun, B.: Spatial variability of surface mass balance along a traverse route from Zhongshan station to Dome A, Antarctica, *Journal of Glaciology*, 57, 658–666, 2011.
- Fujiwara, K. and Endo, Y.: Report of the Japanese Traverse Syowa-South Pole 1968-1969, JARE Scientific Reports, pp. 68–109, 1971.
- Gallée, H., Preunkert, S., Argentini, S., Frey, M. M., Genthon, C., Jourdain, B., Pietroni, I., Casasanta, G., Barral, H., Vignon, E., Amory, C., and Legrand, M.: Characterization of the boundary layer at Dome C (East Antarctica) during the OPALE summer campaign, *Atmospheric Chemistry and Physics*, 15, 6225–6236, 2015.
- Gallet, J. C., Domine, F., Arnaud, L., Picard, G., and Savarino, J.: Vertical profile of the specific surface area and density of the snow at Dome C and on a transect to Dumont D’Urville, Antarctica – albedo calculations and comparison to remote sensing products, *The Cryosphere*, 5, 631–649, 2011.
- Herron, M. M. and Langway, C. C.: Firn Densification: An Empirical Model, *Journal of Glaciology*, 25, 373–385, 1980.
- Kaspers, K. A., van de Wal, R. S., van den Broeke, M. R., Schwander, J., Van Lipzig, N. P. M., and Brenninkmeijer, C. A. M.: Model calculations of the age of firn air across the Antarctic continent, *Atmospheric Chemistry and Physics*, 4, 1365–1380, 2004.
- Kreutz, K., Koffman, B., Breton, D., and Hamilton, G.: Microparticle, Conductivity, and Density Measurements from the WAIS Divide Deep Ice Core, Antarctica, U.S. ANTARCTIC PROGRAM DATA CENTER, 2011.
- Medley, B., Joughin, I., Das, S. B., Steig, E. J., Conway, H., Gogineni, S., Criscitiello, A. S., McConnell, J. R., Smith, B. E., van den Broeke, M. R., Lenaerts, J. T., Bromwich, D. H., and Nicolas, J. P.: Airborne-radar and ice-core observations of annual snow accumulation over Thwaites Glacier, West Antarctica confirm the spatiotemporal variability of global and regional atmospheric models, *Geophysical Research Letters*, 40, 3649–3654, 2013.
- Montgomery, L., Koenig, L., and Alexander, P.: The SUMup Dataset: Compiled measurements of surface mass balance components over ice sheets and sea ice with preliminary analysis over Greenland, *Earth System Science Data Discussions*, pp. 1–31, 2018.
- Sugiyama, S., Enomoto, H., Fujita, S., Fukui, K., Nakazawa, F., Holmlund, P., and Surdyk, S.: Snow density along the route traversed by the Japanese–Swedish Antarctic Expedition 2007/08, *Journal of Glaciology*, 58, 529–539, 2012.
- van den Broeke, M. R., Winther, J.-G., Isaksson, E., Pinglot, J. F., Karlof, L., Eiken, T., and Conrads, L.: Climate variables along a traverse line in Dronning Maud Land, East Antarctica, *Journal of Glaciology*, 45, 295–302, 1999.

Watanabe, O.: Density and hardness of snow in Mizuho Plateau-West Enderby Land in 1970–1971, JARE Data Reports, 27, 187–235, 1975.